X-ray imaging using a tunable coherent X-ray source based on parametric X-ray radiation

2013 JINST 8 C08001

(http://iopscience.iop.org/1748-0221/8/08/C08001)

PUBLISHED BY IOP PUBLISHING FOR SISSA MEDIALAB

RECEIVED: *December 29, 2012*
REVISED: *June 18, 2013*
ACCEPTED: *June 26, 2013*
PUBLISHED: *August 8, 2013*

7th MEDICAL APPLICATIONS OF SYNCHROTRON RADIATION WORKSHOP (MASR 2012)
SHANGHAI SYNCHROTRON RADIATION FACILITY (SSRF),
17–20 OCTOBER, 2012

X-ray imaging using a tunable coherent X-ray source based on parametric X-ray radiation

Y. Hayakawa,[a,1] **Y. Takahashi,**[b] **T. Kuwada,**[c] **T. Sakae,**[c] **T. Tanaka,**[a] **K. Nakao,**[a] **K. Nogami,**[a] **M. Inagaki,**[a] **K. Hayakawa**[a] **and I. Sato**[d]

[a] *Laboratory for Electron Beam Research and Application (LEBRA), Institute of Quantum Science, Nihon University,*
Narashinodai 7-24-1, Funabashi 274-8501, Japan

[b] *Institute of Materials Structure Science, High Energy Accelerator Research Organization (KEK-PF),*
1-1 Oho, Tsukuba, Ibaraki 305-0801, Japan

[c] *School of Dentistry at Matsudo, Nihon University,*
Sakaecho-Nishi 2-870-1, Matsudo 271-8587, Japan

[d] *Advanced Research Institute for the Science and Humanities, Nihon University,*
12-5, Gobancho, Chiyoda-ku, Tokyo 102-8251, Japan

E-mail: yahayak@lebra.nihon-u.ac.jp

ABSTRACT: A novel X-ray source based on parametric X-ray radiation (PXR) has been employed for X-ray imaging at the Laboratory for Electron Beam Research and Application (LEBRA), Nihon University. Notable features of PXR are tunable energy, monochromaticity with spatial chirp, narrow local bandwidth and spatial coherence. Since the X-ray beam from the PXR system has a large irradiation area with uniform flux density, the PXR-based source is suited for X-ray imaging, especially for application to phase-contrast imaging. Despite the cone-like X-ray beam, diffraction-enhanced imaging (DEI) can be employed as a phase contrast imaging technique. DEI experiments were performed using 14- to 34-keV X-rays and the phase-gradient images were obtained. The results demonstrated the capability of PXR as an X-ray source for phase-contrast imaging with a large irradiation field attributed to the cone-beam effect. Given the significant properties of the LEBRA-PXR source, the result suggests the possible construction of a compact linac-driven PXR-Imaging instrument and its application to medical diagnoses.

KEYWORDS: X-ray generators and sources; Accelerator Applications; Computerized Tomography (CT) and Computed Radiography (CR)

[1] Corresponding author.

doi:10.1088/1748-0221/8/08/C08001

Contents

2013 JINST 8 C08001

1 Introduction

Practical X-ray sources have been based on bremsstrahlung and characteristic X-rays since W. Röntgen discovered X-rays in 1895. Synchrotron radiation (SR) has constituted a remarkable innovation in X-rays, and various X-ray techniques have been developed using these advanced sources. However, bremsstrahlung is the physical principle of SR, as of conventional sources, and the large scale of SR facilities restricts the spread of such advanced techniques. In particular, it is difficult to introduce the fruits of the medical application of SR into ordinary clinics. Thus, different mechanisms of X-ray generation have been proposed and studied to realize X-ray sources that can provide advanced applications to clinics [1–4]. Parametric X-ray radiation (PXR), a phenomenon caused by the interaction between a relativistic electron and a crystal medium, is one of the proposed principles for a novel X-ray source [5, 6]. The first PXR source with a dedicated beamline was developed at the Laboratory for Electron Beam Research and Application (LEBRA), at Nihon University [7]. The PXR source operates using an electron beam from a 125-MeV electron linac. So far, X-ray beams of wide tunability have been provided for user applications, primarily X-ray imaging and X-ray absorption fine structure (XAFS) analysis [8, 9].

1.1 Parametric X-ray radiation

PXR is a kind of polarized radiation similarly to Cherenkov radiation and transition radiation, and this phenomenon can be interpreted as Bragg diffraction for virtual photons accompanying the incident electron from the viewpoint of quantum theory [10, 11]. Figure 1 shows a schematic explanation of PXR when an incident electron with the velocity $\boldsymbol{v}$ travels through a crystal medium

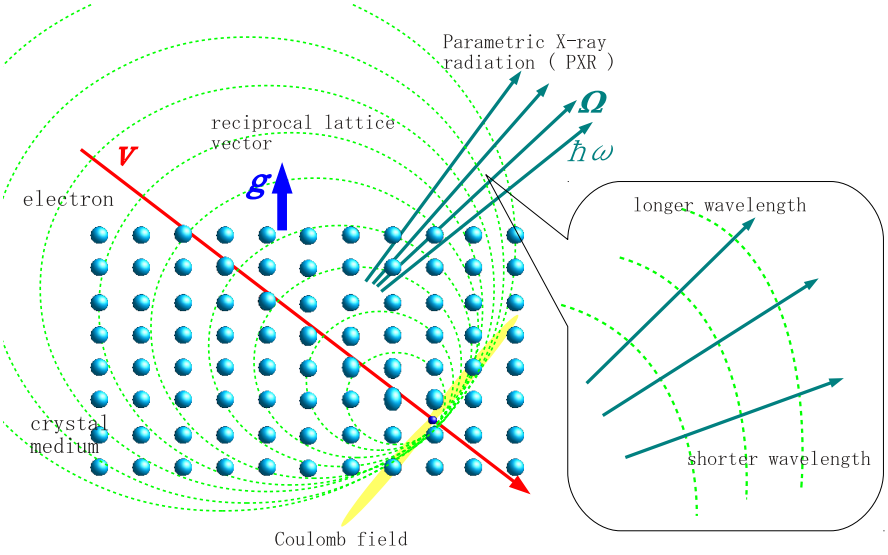

Figure 1. Schematic explanation for PXR as polarized radiation induced by a relativistic electron.

with the reciprocal lattice vector $\boldsymbol{g}$. Each atom excited by the Coulomb field of a relativistic electron emits electromagnetic radiation isotropically. Due to the spatial periodicity of the crystal and the Doppler effect, the wave front is formed like spherical waves, the centers of which slip along the electron track. Taking account of the energy and momentum conservation laws, the energy of PXR emitted along the unit vector Ω is expressed as

$$\hbar\omega \approx \hbar\left(\frac{\omega}{c}\Omega - \boldsymbol{g}\right)\cdot\frac{\boldsymbol{p}c^2}{E} = \frac{\hbar c|\boldsymbol{g}\cdot\boldsymbol{v}|}{c-\boldsymbol{v}\cdot\Omega}, \tag{1.1}$$

where the light speed c in the medium is approximately equal to that in a vacuum, and $\boldsymbol{p}$ and E are the momentum and the energy of the incident electron, respectively [12]. When the incident electron is sufficiently relativistic, the PXR energy is scarcely dependent on the electron energy. On the other hand, the differential cross-section of PXR is given by the perturbation theory and is written as,

$$\frac{\mathrm{d}N}{\mathrm{d}\Omega} = \frac{e^2 n\omega L|\chi_g(\omega)|^2}{2\pi\hbar\varepsilon^3 v(c-\boldsymbol{v}\cdot\Omega)} \times \frac{\left|\frac{\omega}{c}\Omega\times\left(\frac{\omega}{c^2}\boldsymbol{v}+\boldsymbol{g}\right)\right|^2}{\left\{\left|\frac{\omega}{c}\Omega_\perp - \boldsymbol{g}_\perp\right|^2 + \frac{\omega^2}{v^2}\gamma^{-2}\right\}^2}, \tag{1.2}$$

where $\mathrm{d}N$ is the number of quanta emitted in the solid angle $\mathrm{d}\Omega$ when n electrons with charge e, mass m and energy E pass through a crystal with thickness L; $\gamma = E/mc^2$, $v = |\boldsymbol{v}|$; $\Omega_\perp$ and $\boldsymbol{g}_\perp$ are the components of Ω and $\boldsymbol{g}$ perpendicular to $\boldsymbol{v}$, respectively [13]. Finally, the symbol $\chi_g(\omega)$ indicates the Fourier component of the variable part of the dielectric susceptibility. Equation (1.1) and eq. (1.2) can be interpreted as the phase-matching condition of PXR production. Only the radiation within the cone of a $1/\gamma$ radius survives the interference between numerous atoms in the crystal, and every radiation has a wave front of the same form. Although the wave front of PXR is different from both a plane wave and a spherical wave, PXR has intrinsic spatial coherence [14]. In

2013 JINST 8 C08001

the case of using a perfect crystal as radiator, PXR has rather narrow band-width locally [15, 16]. Corresponding to the slight variation of the space of the wave front as shown in figure 1, however, PXR has an energy dispersion, which can be termed spatial chirp, in its radiation cone.

The total probability of PXR emission can be calculated by integrating eq. (1.2); for instance, it is roughly estimated to be 10^{-5} to 10^{-4} photons per one relativistic electron in the case of using a 1-mm-thick Si(111) crystal. The value does not strongly depend on the electron energy but on the property of the crystal medium. Thus, PXR is one of the appropriate X-ray sources for electron accelerators of operation energies less than 1 GeV.

2 LEBRA PXR source

2.1 Double-crystal system

Since the direction of the PXR emission varies depending on the X-ray energy, the problem of the X-ray beam transport had to be solved to realize a PXR-based tunable source. Here, let us consider only the horizontal plane, where θ and ϕ are the Bragg angle of the symmetric Bragg condition and the angle between the electron velocity and the X-ray direction, respectively. Around the Bragg condition $\phi = 2\theta$, a slight difference $\Delta\theta$ of the angle ϕ shifts the PXR energy to

$$\hbar\omega' \approx \hbar\omega + \frac{\mathrm{d}(\hbar\omega)}{\mathrm{d}\phi}\Delta\theta \approx \hbar\omega\left(1 - \frac{\sin 2\theta}{1-\cos 2\theta}\Delta\theta\right) = \hbar\omega\left(1 - \frac{\Delta\theta}{\tan\theta}\right), \tag{2.1}$$

where $\beta = |\boldsymbol{v}|/c \approx 1$ is used in the approximation. Equation (2.1) is an approximate description of the spatial chirp in a PXR beam [17, 18]. On the other hand, the ordinary Bragg energy expressed by $\hbar\omega = \hbar c|\boldsymbol{g}|/2\sin\theta$ is equal to the PXR energy in the case of $\Delta\theta = 0$. The X-ray energy $\hbar\omega''$ that satisfies the Bragg condition for the Bragg angle $\theta + \Delta\theta$ is approximated by

$$\hbar\omega'' \approx \hbar\omega + \frac{\mathrm{d}(\hbar\omega)}{\mathrm{d}\theta}\Delta\theta = \hbar\omega + \frac{\hbar c|\boldsymbol{g}|\cos\theta}{2\sin^2\theta}\Delta\theta = \hbar\omega\left(1 - \frac{\Delta\theta}{\tan\theta}\right). \tag{2.2}$$

The correspondence between $\hbar\omega'$ and $\hbar\omega''$ means that combining the cone-like divergence and the spatial chirp of PXR allows the reflection of the whole of a PXR beam using a double-crystal system in the $(+,-)$ arrangement. Although this analytic approximation is dependent on the equivalence between $|\boldsymbol{v}|$ and c, the results of the numerical simulation based on the ray-tracing method roughly agree with the relation in eq. (2.1) and eq. (2.2) in the case of the electron energy 100 MeV [7]. Thus, the LEBRA-PXR source equipped with a double-crystal system, in which one of the crystals is the PXR radiator and the other is a reflector to transport the PXR beam through a thick shield wall, was developed applying the conventional 125 MeV electron linac as shown in figure 2.

2.2 Specification of the LEBRA-PXR source

The LEBRA linac has typically provided an electron beam at the energy of 100 MeV to work the PXR source [19]. Usually, one 0.2-mm-thick plate and one 5-mm-thick plate of perfect Si crystal are used for the radiator and the reflector, respectively. PXR beams have been produced at the energy range from 5 to 34 keV using Si(111) or Si(220) planes for the LEBRA-PXR source. The actual PXR yield is limited by the maximum reflectance at the peak of the 2nd-crystal rocking curve

2013 JINST 8 C08001

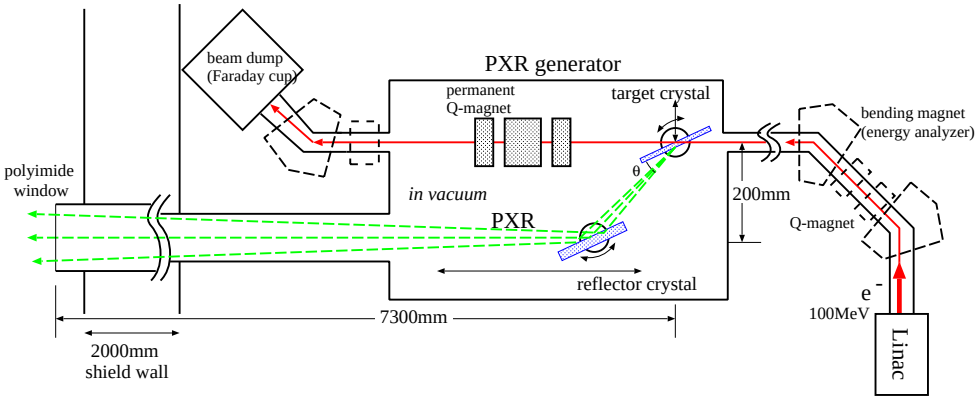

Figure 2. Schematic drawing of the PXR generator with a double-crystal system covering a wide tunability.

Table 1. Typical parameters of the linac and the PXR source of LEBRA.

Electron energy	100 MeV (typ.)
Electron energy spread	$\leqq$ 1 %
Accelerating frequency	2856 MHz (S-band)
Electron bunch length	3 – 10 ps
Macropulse beam current	120 – 135 mA (typ.)
Macropulse duration	4 – 5 μs (typ.)
Macropulse repetition rate	2–5 pps
Normalized emittance	$\sim 15\pi$ mm mrad (rms)
Beam size on the target	0.5 – 2 mm in dia. (fwhm)
Average beam current	1 – 5 μA
PXR energy range	
Si(111) target:	4.0 – 20.5 keV
Si(220) target:	6.5 – 34 keV
Irradiation field at the X-ray exit	100 mm in diameter
Total X-ray photon rate	$\sim 10^7$ /s @17.5 keV

depending on the β value of the incident electron. Taking account of this efficiency and the cutoff effect due to the X-ray transport duct, the available photon rate is typically estimated to be 10^{-8} to 10^{-6} photons per electron in the case of the electron energy of 100 MeV. In a recent work, a Si crystal plate with a wedge-shaped edge was adopted as a PXR radiator to improve the performance of the PXR beam [20–23]. The current specifications of the LEBRA-PXR source are listed in table 1. In our experience, the radiator crystal could be easily destroyed by one macropulse of the electron beam if the macropulse duration is longer than 10 μs [24]. In contrast, no serious destruction was observed at the condition of a macropulse shorter than 5 μs. Thus, the duration of 5 μs and the repetition rate of 5 pps are typically selected for the parameters of the linac macropulse, and the average current of the electron beam is roughly estimated to be 3 μA at the target crystal.

2013 JINST 8 C08001

With respect to the shape of the radiation cone, PXR also depends on the incident electron energy as same as other radiation phenomena caused by relativistic electrons. The aperture angle of the cone, however, is roughly estimated to be $3\gamma^{-1}$ in fwhm. Since the electron energy of the LEBRA system is typically 100 MeV, the PXR beam grows wider than the window 100 mm in diameter at a distance of 7.3 m from the radiator crystal. The actual aperture of the PXR cone extracted to the experiment room is restricted by the exit window to 13.7 mrad. The relatively large aperture allows obtaining a large irradiation area with a short propagation.

3 X-ray imaging using the LEBRA-PXR source

So far, X-ray radiography and XAFS analysis using wide tunability and a locally narrow bandwidth have been popular applications of the LEBRA-PXR source. In addition, the large and flat irradiation area of the PXR beam has encouraged user researchers to perform different studies on X-ray imaging.

3.1 Absorption-based monochromatic imaging

Simple monochromatic X-ray imaging has been carried out at various conditions using PXR tunability. Figure 3 shows a typical example of the results of such experiments. Since the PXR source is a pulsed source and the average photon rate is rather restricted, the measurement typically requires an exposure time from several 10 s to several 10 min [25].

Recently, monochromatic computed tomography (CT) for light materials was successfully performed using the LEBRA-PXR source. Using a high-efficiency flat panel detector (FPD), tomographic images were obtained with total measurement times of 5 min to 1 hour. Figure 4 shows a typical snapshot of such 3D tomography, reconstructed from 180 projections at 17.5 keV. Although the active area of CT measurements is restricted by the detector size to 51.6 mm $\times$ 51.6 mm at present, an irradiation field 100 mm in diameter could be fully utilized with a sufficiently large image sensor [26].

3.2 Diffraction-enhanced imaging

In the case of the ultrarelativistic incident electron, the PXR energy described in eq. (1.1) is substantially independent of the electron energy. The PXR energy observed in a certain solid angle is exactly determined by the geometrical condition of the target crystal, even though the electron beam has a relatively wide energy spread. In addition to the fine energy selection, PXR has an intrinsic spatial coherence due to a periodic structure comparable to an X-ray wavelength. Using an incoherent X-ray source, the spatially coherent region strongly depends on the source size on the basis of the van Cittert-Zernike theorem. Usually, the X-ray source size smaller than several-tens micrometer in diameter is required for X-ray phase-contrast imaging. In the case of the PXR-based source, however, the spatial coherence is available despite the electron-beam spot size of several hundreds micrometer on the target crystal. Thus, X-ray phase-contrast imaging is one of the promising applications of PXR [27–29]. In fact, the edge-enhanced effect resulting from propagation-based phase contrast has been observed at the distance shorter than 10 m from the radiator crystal, though the electron-beam spot on the target crystal usually measures sub-millimeters in diameter [8, 30, 31].

2013 JINST 8 C08001

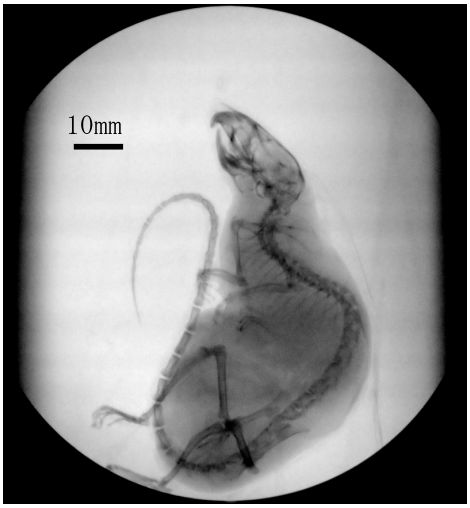

Figure 3. A conventional X-ray image of a mouse observed using 25.5 keV-PXR from Si(220) planes, where the average current of the electron beam was 1.1 μA and the exposure time was 15 min using an imaging plate (IP).

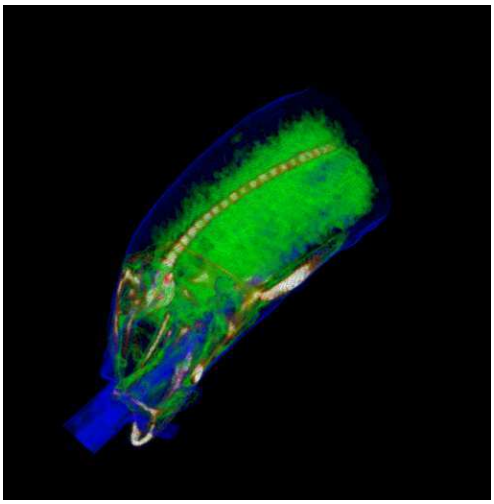

Figure 4. A typical snapshot of 3D tomography for a raw fish sample. The tomogram was reconstructed from 180 projection images taken with 10-s exposures using a 17.5-keV PXR beam and a flat panel detector (FPD), where the average current of the electron beam is 3 μA.

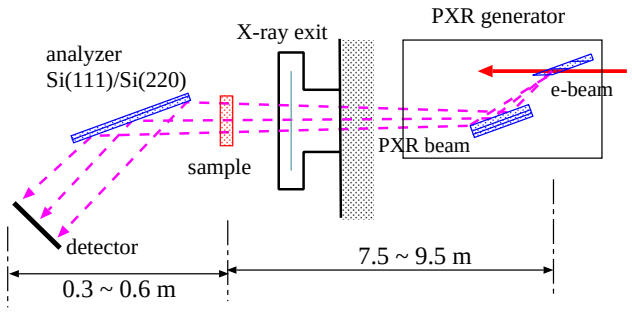

Figure 5. Schematic top view of the setup of the DEI experiment using the LEBRA-PXR source. The same crystal plane as the PXR double-crystal system is used for the analyzer crystal.

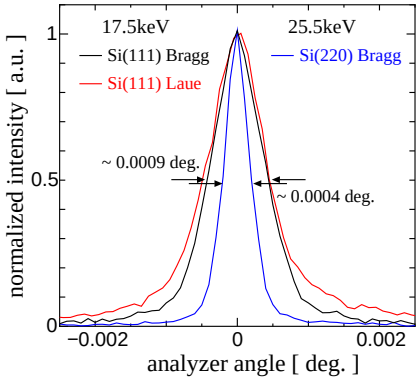

Figure 6. The typical rocking curves observed at the analyzer crystal of the DEI setup.

Furthermore, combining the cone-like divergence and spatial chirp of PXR allows diffraction-enhanced imaging (DEI) using a PXR beam. When an analyzer crystal for DEI (3rd crystal) was set up in the $(+,-,+)$ arrangement as shown in figure 5, eq. (2.1) and eq. (2.2) are also applicable for the diffraction by the analyzer crystal. As shown in figure 6, rocking curves for the whole of the PXR beam observed at the 3rd crystal have almost the same shapes as in the case of plane-wave-like X-ray beams. Here, the actual aperture is restricted by the size of the analyzer crystal plate. For instance, the horizontal aperture angle is estimated to be approximately 1.2 mrad in the case of the black solid curve shown in figure 6, where a 110 mm $\times$ 100 mm Si(111) crystal plate was used

2013 JINST 8 C08001

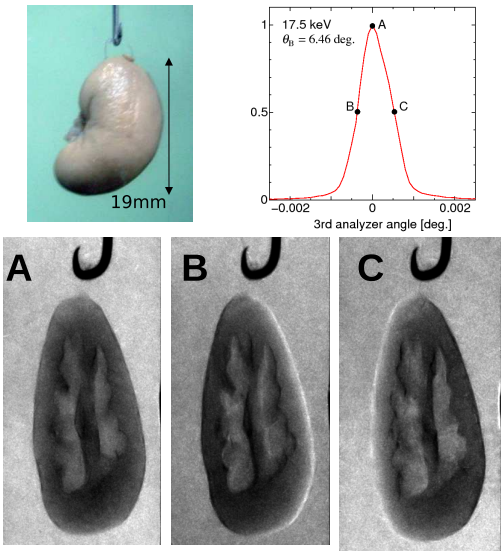

Figure 7. Typical DEI images of a mouse kidney obtained at analyzer angles marked A, B and C on the rocking curve, where the PXR energy was 17.5 keV and a 5-mm-thick Si(111) crystal in a Bragg case was used for the analyzer.

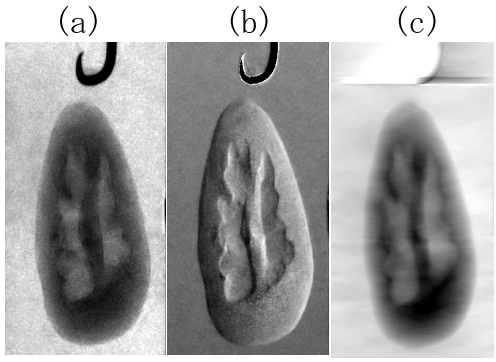

Figure 8. (a) The absorption-contrast image obtained as the sum of the DEI images B and C in figure7. (b) The phase-gradient map obtained as the image calculation (B−C)/(B+C) [35]. (c) The result of the phase retrieval by spatially integrating the phase-gradient map (b).

for the analyzer in a Bragg case at the distance of 10 m from the radiator crystal. The diffraction widths for the PXR beam, which are much narrower than the cone-beam aperture, mean that DEI with angular resolution of 10^{-6} rad is possible using PXR.

DEI experiments using the LEBRA-PXR source were successfully carried out under various conditions in the X-ray energy range from 14 to 34 keV using the experimental setup Fig 5 [32, 33]. Figure 7 shows typical DEI images using PXR. Each DEI image was taken with an exposure time of 60 s using an X-ray CCD when the average current of the electron beam was 2.6 μA. Here, the meaning of the PXR energy is the X-ray energy at the horizontal center in the radiation cone having the spatial chirp. In the case of the 17.5 keV PXR beam from Si(111) planes, the energy dispersion of the spatial chirp is estimated to be approximately 154 eV/mrad using eq. (2.1). From these DEI images, a phase-gradient map can be obtained as well as an absorption-contrast one by the image calculations as shown in figure 8 [34]. The phase map retrieved from the phase-gradient map is also shown in figure 8 (c).

The spatial coherence of the PXR beam is strongly dependent on the geometrical condition of the target crystal as the radiator. When the target crystal has multiple surfaces as PXR exits, the spatial coherence of the available PXR beam is destroyed by superposition of different X-ray beams [22, 23]. On the other hand, electron beam size on the target crystal is not a significant matter for the spatial coherence of PXR. Of course, an electron beam size larger than several millimeters is an unfavorable factor because the effect of the deformation of the thin target crystal is not negligible. On the whole, an electron beam smaller than 1 mm in diameter is not a problem for DEI using the LEBRA-PXR source. Thus, shorter X-ray wavelengths do not mean the reduction of the coherent region even though the electron beam size remains unchanged. Special improvements

2013 JINST 8 C08001

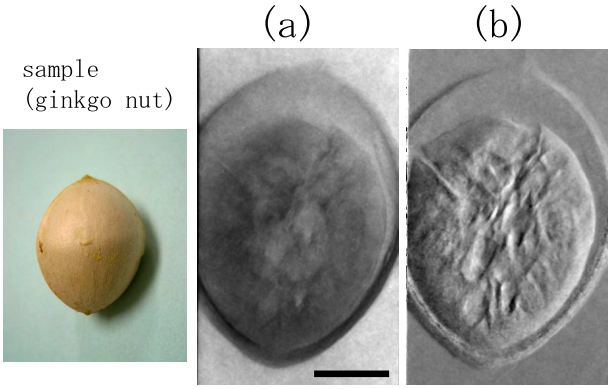

Figure 9. The typical result of a DEI experiment for a ginkgo nut using a 25.5 keV-PXR beam. (a) Absorption-contrast and (b) phase-gradient images calculated from 2 DEI images obtained with exposures of 30 min. The scale bar indicates 5 mm.

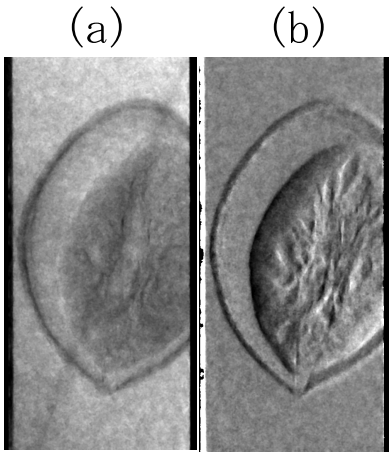

Figure 10. (a) Absorption-contrast and (b) phase-gradient images calculated from 2 DEI images obtained with exposures of 20 min using the 34 keV-PXR beam.

in the performance of the electron beam are not necessary to allow DEI at the higher X-ray energy. In fact, phase-gradient maps of DEI at the region of X-ray energy higher than 20 keV were obtained using an Si(220) $(+,-,+)$ system without extremely focusing the electron beam. Figure 9 shows a typical result of the DEI experiments using a 25.5 keV PXR beam when the electron beam was 1.1 μA and the sample was a ginkgo nut. The result of using a 34 keV PXR beam is also shown in figure 10, where the conditions except the PXR energy and the exposure time were the same as in figure 9. These results were obtained using the electron beam of which spot size on the target crystal was roughly estimated to be 0.5 mm or more in fwhm diameter. Here, both the available photon rate diffracted from the 2nd crystal in the PXR generator and the quantum efficiency of the X-ray CCD used in these experiments considerably fall as the X-ray energy increases. In particular, a drop in the efficiency of X-ray absorption in the scintillator layer (20 μm-thick P43) of the X-ray CCD is considerably serious; for instance, the efficiency for 34keV X-rays is estimated to be 5 % at most. The effective quantum-efficiency of the imaging device may get worse owing to the capability of the image intensifier and the coupling lens system. Therefore, a long exposure time of several ten minutes was required for each DEI image to improve the S/N ratio.

3.3 PXR-DEI using a Laue-case analyzer

Due to the extension of the cone-beam, a significantly wider irradiation field could be obtained from the LEBRA-PXR source without asymmetric reflection. An irradiation field 100 mm in diameter is available at the X-ray exit window 7.3 m distant from the target crystal as the PXR radiator. Due to the radiation cone with the aperture angle of 13.7 mrad. the irradiation field grows larger downstream of the exit window. Essentially, such a large area could be fully utilized for DEI at a distance between the PXR source and the sample shorter than 10 m. At present, however, the active area for DEI is restricted by the size of the analyzer crystal and the detector size. Since the

2013 JINST 8 C08001

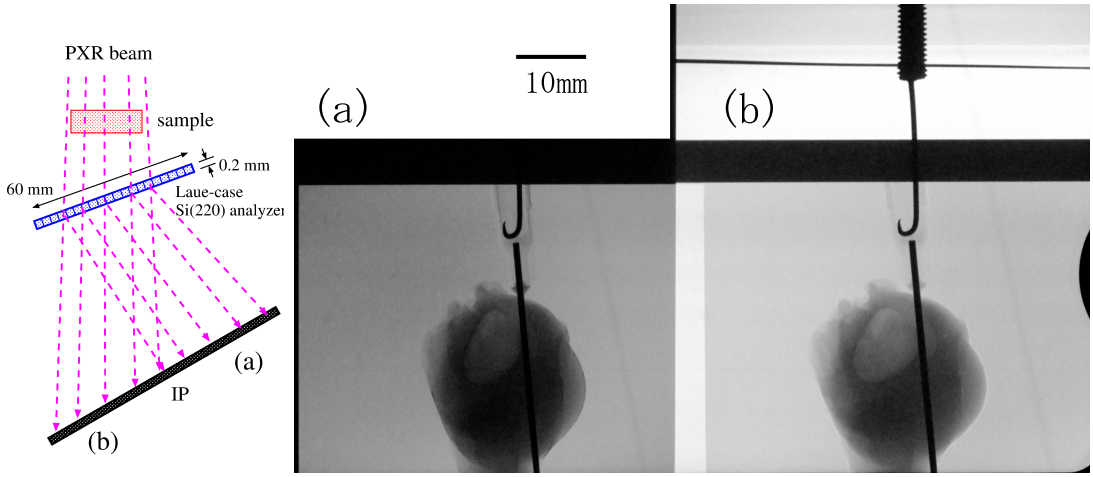

Figure 11. The result of the DEI experiment using an analyzer crystal of Si(220) in the Laue case, where the sample was a pig eyeball and the PXR energy was 17.5 keV. (a) The diffracted image; (b) the forward image. The exposure time was 10 min using an IP when the average beam current was 2.7 μA.

maximum length of our analyzer crystal in the Bragg case was 110 mm, the width of the active area was approximately 12 mm in the case of the Bragg angle of 6.5°.

In contrast, an analyzer crystal in the Laue case has an advantage in the effective area [31, 36, 37]. Thus, a DEI experiment where a Laue-case analyzer was used for the 3rd crystal was performed using a 17.5-keV PXR beam from the Si(220) system. The result of the experiment is shown in figure 11, where a pig eyeball was used for the sample. The diffracted image and the forward image were simultaneously taken using a panorama IP. Although shadings probably due to crystal deformations were observed, an active area of at least 50 mm $\times$ 50 mm was available. The active area corresponds to the 5 mrad aperture angle of the cone-beam actually used in this measurement. The result suggests that DEI experiments with the irradiation field larger than 100 mm in diameter are not difficult if we can prepare a sufficiently large analyzer crystal without deformations.

4 Discussion on the improvement of the PXR intensity

LEBRA is the medium-scale linac facility attached to a private university, and the PXR source was developed to use for basic science researches [7, 24]. The present LEBRA-linac is pulsed one with a low repetition rate as ahown in figure 12, and its average beam current is limited to a few micro-amperes. The limitation is due to the performance of our RF devices such as klystrons and the protection for the radiation from mainly the beam dump. Since the PXR intensity depends on the beam current of the accelerator, the LEBRA-PXR source may have a great advantage in the time-domain measurement using the micro- or pico-second pulse structure. For practical medical applications of PXR, however, the average beam current of the LEBRA-linac is obviously insufficient. Thus, a novel high duty electron accelerator is required for such applications. Considering recent accelerator technologies, it is not difficult to develop a 100-MeV electron linac with an electron beam of several hundred micro-amperes on average. If an ideal imaging device having high quantum efficiency can be used, a 50-μA linac might be sufficient for a PXR source for mammography.

2013 JINST 8 C08001

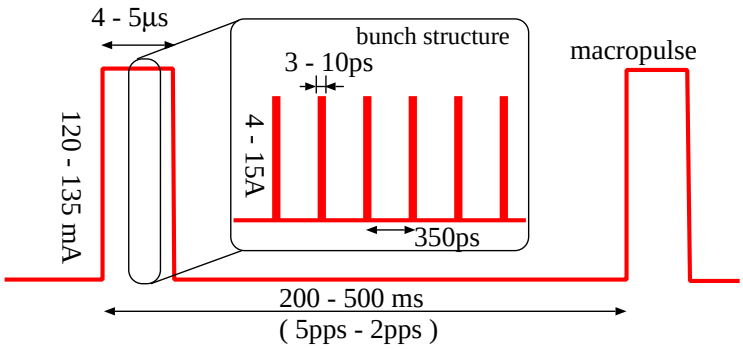

Figure 12. Schematic explanation of the pulse structure of the electron beam at the LEBRA-PXR source.

The destruction of the target crystal bombarded with a high-current electron beam seems to be one of the most serious problems. In the LEBRA-PXR system, a 0.2 mm thick Si crystal in the Bragg case is typically used as the target, and the effective thickness of the target the electron beam penetrates is changed from 0.5 mm to 2 mm depending on the Bragg angle. In the case of a thin silicon medium, the energy deposition by a 100-MeV electron is estimated to be approximately 0.4 MeV per 1 mm thickness. Therefore, the average thermal load on the target of the present PXR source is estimated to be 2.4 W at most when the electron beam current is 3 μA on average. If an average beam current of 200 μA corresponding to a beam power of 20 kW is achieved, the average thermal load of 160 W can be solved using a conventional cooling system. Considering the peak current of electron bunch, the thermal load in pico-second region is on the order of magnitude of MW. So far, however, there has been no problem caused by such prompt heating. In contrast, we have found that the heating during the macropulse corresponding to approximately 50 kW load causes the destruction of the target crystal locally. When the macropulse duration exceeds 10 μs, it has been observed that one macropulse destroys the target crystal [24]. Therefore, it is expected that a linac for a practical PXR source provide macropulses at a high repetition rate of several hundred pps to achieve an beam current higher than 100 μA on average.

Finally, it is supposed that the protection for the background radiation from the beam dump would be the most difficult problem in the realization of a medical PXR source. Since the electron energy required for the PXR source exceeds the threshold for neutron production, a huge volume of neutron shielding will be necessary to protect patients and medical staff. When the entire energy of a 20 kW electron beam is dumped into a graphite block, the neutron yield produced at the beam dump is estimated to be 6×10^{12} n/s [38]. Without effective shield for neutron, there are fears that the dose-equivalent measured at 1 m from the beam dump exceeds 50 Sv/h. The development of an energy-recovery system might be a powerful solution to reduce the volume of necessary radiation shield [39]. Since the purpose of energy recovery is not the reduction of the power consumption, a super-conducting system is not indispensable for the energy-recovery system.

2013 JINST 8 C08001

5 Summary

A PXR-based X-ray source has been kept in working order using a 100-MeV electron beam from the linac at the LEBRA, Nihon University. Various studies on X-ray imaging were carried out using the LEBRA-PXR source. In particular, combining the cone-like divergence and the spatial chirp of PXR allowed DEI using a PXR beam in the $(+,-,+)$ arrangement. PXR-DEI experiments have been successfully performed as one of the most significant applications of the LEBRA-PXR source. At least, DEI with a cone-beam aperture of 5 mrad was achieved using the Si(220) analyzer in the Laue case. The results of the DEI experiments suggest that the spatial coherence of the PXR beam is sufficiently good at X-ray energies higher than 30 keV though the electron beam diameter at the radiator crystal has been estimated to be larger than at least several hundred microns in fwhm.

Since a substantially large irradiation area is easily available with a short propagation distance from the source due to the cone-beam effect, PXR allows relatively compact linac-driven sources with the capability of diffraction-based phase-contrast imaging. For practical medical diagnoses, the linac has to provide a 100-MeV electron beam of several hundred micro-amperes on average. Recent accelerator technologies might allow for such a compact linac except for the problem of shielding the background radiation from the beam dump [40].

Acknowledgments

This work was partly supported by MEXT. KAKENHI (21560055, 24560069 and 24651105) and by Grants-in-Aid for Scientific Research, Nihon University (S09-024, Toshiro Sakae).

References

[1] R. Kuroda et al., *Quasi-monochromatic hard X-ray source via laser Compton scattering and its application*, *Nucl. Instrum. Meth.* **A 637** (2011) S183.

[2] P. Oliva et al., *Start-to-end simulation of a Thomson source for mammography*, *Nucl. Instrum. Meth.* **A 615** (2010) 93.

[3] M. Bech et al., *Hard X-ray phase-contrast imaging with the Compact Light Source based on inverse Compton X-rays*, *J. Synchrotron Rad.* **16** (2009) 43.

[4] W. Wagner, B. Azadegan, M. Sobiella, J. Steiner, K. Zeil and J. Pawelke, *An intense channeling radiation source*, *Nucl. Instrum. Meth.* **B 266** (2008) 327.

[5] V.G. Baryshevsky and I.D. Feranchuk, *A comparative analysis of various mechanisms for the generation of X-rays by relativistic particles*, *Nucl. Instrum. Meth.* **A 228** (1985) 490.

[6] M.A. Piestrup et al., *A design of mammography units using a quasimonochromatic x-ray source*, *Rev. Sci. Instrum.* **72** (2001) 2159.

[7] Y. Hayakawa, I. Sato, K. Hayakawa and T. Tanaka, *Simulations to the project of a PXR based X-ray source composed of an electron linac and a double-crystal system*, *Nucl. Instrum. Meth.* **B 227** (2005) 32.

[8] Y. Hayakawa et al., *Status of the parametric X-ray generator at LEBRA, Nihon University*, *Nucl. Instrum. Meth.* **B 252** (2006) 102.

2013 JINST 8 C08001

[9] A. Mori et al., *Dispersive XAFS Image Radiograph by Parametric X-ray Radiation*, *AIP Conf. Proc.* **879** (2007) 1841.

[10] M.L. Ter-Mikaelian, *High-energy electromagnetic processes in condensed media*, Wiley-Interscience, New York U.S.A. (1972).

[11] Y.N. Adishchev, V.A. Verzilov, A.P. Potylitsyn, S.R. Uglov and S.A. Vorobyev, *Measurement of spectral and polarization characteristics of parametric X-rays in a Si Crystal*, *Nucl. Instrum. Meth.* **B 44** (1989) 130.

[12] A.V. Shchagin, V.I. Pristupa and N.A. Khizhnyak, *A fine structure of parametric X-ray radiation from relativistic electrons in a crystal*, *Phys. Lett.* **A 148** (1990) 485.

[13] H. Nitta, *Kinematical theory of parametric X-ray radiation*, *Phys. Lett.* **A 158** (1991) 270.

[14] V.G. Baryshevsky, I.D. Feranchuk and A.P. Ulyanenkov, *Parametric X-Ray Radiation in Crystals: Theory, Experiment and Application*, *Springer Tracts in Modern Physics* vol 213, Springer Berlin Heidelberg, Berlin/Heidelberg Germany (2005).

[15] K.-H. Brenzinger et al., *How Narrow is the Linewidth of Parametric X-Ray Radiation?*, *Phys. Rev. Lett.* **79** (1997) 2462.

[16] M. Inagaki et al., *Wavelength Dispersive X-ray Absorption Fine Structure Imaging by Parametric X-ray Radiation*, *Jpn. J. Appl. Phys.* **47** (2008) 8081.

[17] Y. Hayakawa et al., *Tunable Monochromatic X-ray Source Based on Parametric X-ray Radiation at LEBRA, Nihon University*, *AIP Conf. Proc.* **879** (2007) 123.

[18] Y. Hayakawa et al., *Advanced Applications of PXR at LEBRA, Nihon University*, *Proc. SPIE* **6634** (2007) 6634111.

[19] T. Tanaka et al., *Performance and Application of FEL and PXR Sources at Nihon University*, *AIP Conf. Proc.* **1234** (2010) 587.

[20] I.D. Feranchuk and S.I. Feranchuk, *Grazing incidence parametric X-ray radiation from the relativistic electron beam moving in parallel to the superlattice surface*, *Eur. Phys. J. Appl. Phys.* **38** (2007) 135.

[21] S.V. Blazhevich and A.V. Noskov, *The Borrmann effect in parametric X-radiation under asymmetric reflection conditions*, *Nucl. Instrum. Meth.* **B 266** (2008) 3777.

[22] Y. Hayakawa et al., *Geometrical effect of target crystal on PXR generation as a coherent X-ray source*, *Int. J. Mod. Phys.* **A 25** (2010) 174.

[23] Y. Hayakawa et al., *Improvement in the performance of the X-ray source based on parametric X-ray radiation using a wedge-shaped target crystal*, *Nuovo Cim.* **C 34** (2011) 253.

[24] Y. Hayakawa et al., *Present status of the parametric X-ray generator at LEBRA* (in Japanese), in *Proceedings of the 1st Annual Meeting of Particle Accelerator Society of Japan and the 29th Linear Accelerator Meeting in Japan*, Funabashi, Japan, pp. 60–62 (2004), http://www.pasj.jp/web_publish/pasj1_lam29/WebPublish/4B05.pdf.

[25] T. Sakae et al., *A Preliminary Study on Low-dose X-ray Imaging Using Parametric X-ray*, *J. Hard Tissue Biol.* **20** (2011) 31.

[26] Y. Hayakawa et al., *Computed tomography for light materials using a monochromatic x-ray beam produced by parametric x-ray radiation*, Submitted to Nucl. Instrum. Meth. B.

[27] T.J. Davis, D. Gao, T.E. Gureyev, A.W. Stevenson, and S.W. Wilkins, *Phase-contrast imaging of weakly absorbing materials using hard X-rays*, *Nature* **373** (1995) 595.

2013 JINST 8 C08001

[28] R. Fitzgerald, *Phase-Sensitive X-Ray Imaging*, *Phys. Today* **53** (2000) 23.

[29] A. Momose, *Recent Advances in X-ray Phase Imaging*, *Jpn. J. Appl. Phys.* **44** (2005) 6355.

[30] Y. Hayakawa et al., *Dependence of PXR beam performance on the operation of the pulsed electron linac*, *Nucl. Instrum. Meth.* **B 266** (2008) 3758.

[31] Y. Takahashi et al., *Phase-contrast imaging with a novel X-ray source*, *AIP Conf. Proc.* **1221** (2010) 119.

[32] T. Kuwada et al., *Phase Contrast Imaging of Biological Materials using LEBRA-PXR*, *AIP Conf. Proc.* **879** (2007) 1968.

[33] T. Sakae et al., *Diffraction Enhanced Phase contrast Imaging of a Kitten Deciduous Tooth using Coherent X-ray Source*, *J. Hard Tissue Biol.* **19** (2010) 131.

[34] Y. Takahashi et al., *Parametric X-ray radiation as a novel source for X-ray imaging*, *X-Ray Spectrom.* **41** (2012) 210.

[35] D. Chapman et al., *Diffraction enhanced x-ray imaging*, *Phys. Med. Biol.* **42** (1997) 2015.

[36] D. Chapman et al., *Mammography imaging studies using a Laue crystal analyzer*, *Rev. Sci. Instrum.* **67** (1996) 3360.

[37] D. Shimao, K. Mori, H. Sugiyama and K. Hyodo, *Imaging of Ligament and Articular Cartilage Due to Refraction-Contrast Using a Laue Geometry Analyzer Crystal*, *Jpn. J. Appl. Phys.* **42** (2003) 5874.

[38] W.P. SWANSON, *Radiological safety aspects of the operation of electron linear accelerators*, Tech. Rep. 188, Inernational atomic energy agency (1979).

[39] R. Hajima, *Energy recovery linacs for light sources*, *Rev. Accl. Sci. Tech.* **03** (2010) 121.

[40] T. Inagaki et al., *C-band linac in scss prototype accelerator of the japanese x-fel project*, in *IEEE Particle Accelerator Conference* (2007) pp. 2766–2768.

2013 JINST 8 C08001